Published as *Physica A*, **239**, 189 (1997), see also http://mobydick.physics.utoronto.ca

Electroconvection patterns in smectic films at and above onset

Samuel S. Mao and John R. de Bruyn

Department of Physics, Memorial University of Newfoundland, St. John's, Newfoundland, Canada A1B 3X7

Stephen W. Morris

Department of Physics and Erindale College, University of Toronto, 60 St. George St., Toronto, Ontario, Canada M5S 1A7

Abstract

We have studied patterns of electrically-driven convective vortices in thin freely-suspended films of smectic liquid crystal at and above the onset of convection. We present measurements of the convective amplitude above onset, the spatial variation of the amplitude due to the presence of end walls, and the relaxation of the amplitude following a sudden change in the experimental control parameter. Our experimental results are shown to agree with predictions based on the Ginzburg-Landau equation, and we find values for the dimensionless length and time scales of the Ginzburg-Landau equation.

I. INTRODUCTION

A dissipative nonlinear system driven out of equilibrium can undergo a bifurcation from a state which is spatially uniform to one which displays ordered spatial or spatio-temporal structure. The structured state is referred to as a pattern [1]. Patterns occur in a variety of

very different systems, including fluid dynamical systems [2], granular materials [3], reacting chemical systems [4], and slime mold colonies [5]. In many cases, features of the patterns, and of the pattern-forming bifurcations, are universal in the sense that their characteristics and behaviour are independent of the nature of the underlying physical system [1].

It is very often useful to describe the behaviour of a pattern in terms of an appropriately defined complex amplitude $A(x,t)$, rather than using the equations which describe the dynamics of the underlying system. One manifestation of the universality mentioned above is that the same form of amplitude equation can describe patterns in a wide variety of systems, related only by their symmetries. For example, starting from the Navier-Stokes equations, coupled to an equation for heat transport, Newell and Whitehead [6] and Segel [7] derived an amplitude equation for Rayleigh-Bénard convection (RBC) in a thin fluid layer heated from below. Here the amplitude of the pattern was related to the amplitude of the fluid flow velocity in the pattern of convective rolls that develops when the temperature difference across the fluid layer is large enough. The derivation involved a multiple-scale perturbation analysis, and is valid close to the onset of convection and for an amplitude which varies slowly in space and time. A similar equation can be derived from symmetry considerations [8]. For one-dimensional patterns, the amplitude equation in both cases reduces to the Ginzburg-Landau equation,

$$\tau_0 \frac{\partial A}{\partial t} = \epsilon A - g|A|^2 A + \xi_0^2 \frac{\partial^2 A}{\partial x^2}. \tag{1.1}$$

Here ϵ is the system's control parameter. ξ_0 and τ_0 are characteristic length and time scales over which changes in the amplitude A occur, and can be calculated from the linearized equations of motion of the system; g is a nonlinear coupling parameter.

The Ginzburg-Landau equation (GLE), Eq. (1.1), has been used extensively in the study of one-dimensional patterns, both in cases where it has been rigorously derived from the governing equations of the system (RBC [6,7] and Taylor vortex flow (TVF) [9]), and in cases where it is used simply as a reasonable phenomenological model (e.g., Eckmann vortex flow [10]). In many cases, the predictions of the GLE and the experimental results

agree quantitatively. A clear and accessible review of the application of the GLE to pattern formation in fluid systems is given in Ref. [11].

The bulk of this paper is concerned with the use of the GLE to analyze one dimensional electrically-driven convection patterns in very thin, freely-suspended films of smectic-A liquid crystal [12–16]. In the remainder of this section, we briefly review the properties of the GLE. In Section 2 we describe our experimental system, apparatus and procedures. Our results are presented in Section 3, while Section 4 contains a short discussion.

Eq. (1.1) always has a steady state solution (i.e., with $\partial A/\partial t = 0$) $A = 0$, corresponding to the spatially uniform base state. At $\epsilon = 0$ the base state becomes unstable, and two new solutions appear via a supercritical bifurcation. They have amplitudes $A_0 = \pm\sqrt{(\epsilon - \epsilon_m)/g}$, and correspond to two equivalent patterns related by symmetry. The marginal stability boundary $\epsilon_m(k)$, where k is the wave number of the pattern, can be found by a linear stability analysis of Eq. (1.1) to be $\epsilon_m = \xi_0^2(k - k_c)^2$. Here k_c is the wave number of the pattern state which becomes stable at $\epsilon = 0$. For a pattern with $k = k_c$, the amplitude grows like

$$A = \pm\,(\epsilon/g)^{1/2}\,. \tag{1.2}$$

In a finite system, the boundary conditions on the A can affect both the spatial variation of the pattern amplitude and the stability range of the pattern [17]. Our system, described below, has rigid end walls at which the fluid flow velocity, which is directly related to A, must go to zero. This boundary condition requires that A vary with position along the length of the film. Eq. (1.1) can be solved in a semi-infinite domain to find steady-state solutions with the boundary condition $A = 0$ at $x = 0$. Assuming that $k = k_c$, the result is

$$A = (\epsilon/g)^{1/2}\tanh\left(\frac{x}{\sqrt{2}\xi}\right). \tag{1.3}$$

Here ξ is the length scale over which the amplitude grows from zero at the boundary to its value in the bulk of the system, and is given by

$$\xi = \xi_0\epsilon^{-1/2}. \tag{1.4}$$

ξ diverges as $\epsilon \to 0$. Eq. (1.3) can be applied at each end of a finite system, as long as $\xi \ll \ell$, where ℓ is the length of the system. Eqs. (1.3) and (1.4) agree well with measurements made on RBC [19].

Eq. (1.1) also describes the relaxation of $A(x,t)$ towards a steady state. Considering a region of the pattern where any spatial variation of A can be neglected, Eq. (1.1) can be solved to give

$$A(t) = \left(\frac{(\epsilon A_i^2/g)\, e^{2t/\tau}}{(\epsilon/g) - A_i^2\,(1 - e^{2t/\tau})} \right)^{1/2}. \tag{1.5}$$

Here A_i is the initial amplitude at $t = 0$. τ is the time scale over which the amplitude relaxes and is given by

$$\tau = \tau_0 \epsilon^{-1}. \tag{1.6}$$

Thus τ also diverges as $\epsilon \to 0$. These predictions are in good agreement with the results of experiments on RBC [18,19] and TVF [20].

II. EXPERIMENT

The experimental system we have studied consists of a very thin film of smectic-A liquid crystal supported only at its edges (i.e., with two free surfaces) [12,13]. The liquid crystal used was 4,4′-n-octylcyanobiphenyl (8CB) doped with $(7.5 \pm 0.2) \times 10^{-3}$ mol/l tetracyanoquinodimethane (TCNQ) to control the nature of the ionic species in the material. 8CB is composed of rod-shaped molecules. In the smectic-A phase the molecules are arranged in layers with their long axes aligned in the direction of the layer normal [21]. The thickness of a single smectic layer is 3.16 nm. As a result of this layered structure, freely suspended films a small number of molecular layers thick can be made. These films are very stable, and with practice can be made uniformly thick. Flow in a film is entirely in the plane of the film, and, fluid dynamically, a smectic film behaves as a two-dimensional isotropic fluid [13]. When a sufficiently high voltage is applied across the film, a periodic pattern of convective vortices develops along the length of the film [12].

The experimental set up used in the present work was a modified version of that used previously [12,13]. The films studied were rectangular. The long sides of the film were supported by two 23 μm-diameter tungsten wires, which also served as electrodes. The ends of the film were supported by thin plastic wipers which rested on the wires. The film holder is shown in Fig. 1. We define x to be the coordinate parallel, and y the coordinate perpendicular to the electrodes. The position of one of the end wipers was fixed, while the other could be driven with a motorized micrometer, allowing variation of the film length ℓ in the range $0 < \ell < 30$ mm. The electrode wires were held by plexiglass yokes, and their separation d could be varied by moving one of the yokes using a fine adjustment screw. In the work reported here, the film width d was between 0.66 mm and 2.0 mm.

Films were made by bringing the two wipers together, placing a small amount of liquid crystal on the place where they joined, and then slowly drawing them apart. Normally, the films will initially be nonuniform in thickness. Since the film thickness s is on the order of a wavelength of visible light, the films show bright interference colours when viewed in reflected white light. Steps in film thickness of a single smectic layer are easily visible to the eye as a change in film colour. The films can be made uniformly thick — and so uniformly coloured — by repeatedly increasing and decreasing the film length, with and without convection present, and can maintain their uniform thickness even in the presence of strong convection.

Voltages of $+V/2$ and $-V/2$ were applied to the two electrodes by means of two HP6024A power supplies wired in series. V is therefore the total voltage applied across the film. When V was increased, a steady, one-dimensional array of counter-rotating convection vortices appeared at a well-defined critical voltage V_c [12]. This pattern persists up to a certain voltage, beyond which the flow becomes unsteady.

The film holder was enclosed in a grounded aluminum housing with optical access. This housing was itself placed in a plexiglass box, the temperature of which was controlled to ± 0.1 °C over a given run using an Omega CN9000A temperature controller. All runs were performed at temperatures in the range 25 ± 1 °C, which is well below the smectic-A–nematic transition at 33 °C.

Our measurements were made by visualizing the flow in the convecting films. The films were viewed through a microscope with a colour ccd video camera. Incense smoke was allowed into the experimental housing, and a small number of smoke particles settled on the film. These were made visible by shining a collimated beam of white light onto the film from below, at an angle slightly off the vertical. When convection was present, the smoke particles were advected by the flow. The flow pattern was recorded on video tape and the video data analyzed after the fact. The pattern's wavelength could be measured directly from a video monitor, while flow velocities could be obtained by tracking the motion of the particles.

Since the onset voltage V_c depends on the film thickness s, it is important to measure s accurately. We did this using two different techniques. The first involves colourimetry. The colour of the film as it appears in reflected white light is due to the interference of light reflected from its upper and lower surfaces, and so depends on film thickness. This colour can be calculated in terms of the CIE chromaticity diagram [22]. The calculation takes into account the optical properties of the film, the spectral distribution of the light source, and the spectral response of the human eye [23]. The result is shown in Fig. 2. With practice, s can be determined from a film's colour by eye, with an accuracy of plus or minus one or two smectic layers, for films up to about 100 layers thick.

We also determined s from reflectivity measurements [24]. A 6328Å laser beam, polarized perpendicular to the plane of incidence, was directed onto the film at an angle of incidence of 45°. The incident intensity was monitored with a beam splitter and a calibrated photodiode detector, and the intensity of the light reflected from the film was measured with an identical detector. The film thickness was found by comparing the measured reflectivity with that calculated as described in Ref. [25]. Although the reflectivity is periodic in s, if a film's thickness is known approximately either from its colour or from a measurement of V_c (see below), then the thickness can be determined quite accurately. For $s \lesssim 10$ layers, the change in reflectivity due to a one-layer change in s is large compared to the experimental uncertainties and the thickness determination using this method is exact. For films between

10 and 100 layers thick, the combination of the reflectivity and colour measurements allowed determination of s with an accuracy of ± 1 layer.

III. RESULTS

In this section we present experimental results on electroconvection in smectic-A films at and above the onset of convection. Our results are analyzed in terms of the GLE, Eq. (1.1). In particular, the amplitude of the pattern above onset, its spatial variation, and the way in which the amplitude evolves to a steady state are all found to agree with the predictions of the GLE. Our results allow us to obtain values for the length and time scales ξ_0 and τ_0, as well as the nonlinear parameter g.

A. Onset voltage

The voltage at the onset of convection was measured in the earlier version of this experiment [12]. The electrode configuration was somewhat different in that apparatus, and the measurements were done on films of thicker than about 40 molecular layers. Here we extend the measurements down to films as thin as two layers thick.

The onset voltage V_c is determined by observing the motion of flow visualization particles as the magnitude of the applied field is slowly increased or decreased. V_c is taken to be the lowest value of the voltage across the film for which an organized pattern of vortices exists throughout the entire length of the film. Within the measurement uncertainties, no hysteresis was observed in the threshold voltage.

Fig. 3 shows V_c as a function of film thickness for several films of the same length and width. The data points represent an average over several measurements in films of the same thickness. For thin films the data are linear, but for $s \gtrsim 25$ layers V_c increases more slowly. Fig. 4 shows data for thin films of three different aspect ratios. The data extend down to s as small as 2 smectic layers and show no dependence on film width. The intercept at

vanishing film thickness is not significantly different from zero, and a fit through the origin to all three sets of data shown yields

$$V_c = (1.05 \pm 0.01)s, \tag{3.1}$$

where V_c is in Volts and s in molecular layers.

The measurements of film thickness, discussed above, are more precise than the measurements of V_c, which rely on a subjective observation of the flow pattern in the film. Because of this, in the results presented below, we calculated V_c from the measured value of s, using Eq. (3.1) for thin films and a smooth curve through the $V_c(s)$ data for thicker films.

B. Critical wave number

The wave number k of the pattern can be determined by counting the number of vortex pairs along the film. For a regular pattern containing N vortices, or P pairs where $P = N/2$, the average wave number is given by $k = 2\pi P/l$. Fig. 5 shows P_c, the number of vortex pairs in the pattern at onset, as a function of aspect ratio $\Gamma = l/d$. The thickness of the films in Fig. 5 varies from 2 to 75 molecular layers; no dependence of the data on s is observed. Due to the finite length of the film, N is quantized, since there must be an integer number of vortices along the length of the film, and this is reflected in the small scatter in the data shown in Fig. 5. A linear fit through the origin gives $P_c = (0.786 \pm 0.004)\,\Gamma$, from which we find

$$k_c = (4.94 \pm 0.03)\, d^{-1}. \tag{3.2}$$

or equivalently, $\lambda_c = (1.27 \pm 0.01)\, d$. This result agrees with the value of $\lambda_c = (1.30 \pm 0.05)\, d$ found from our earlier measurements [12].

Above onset, the wave number of the pattern can change due to vortices being created or destroyed. Our results on wave number selection above onset are reported elsewhere [14].

C. Bifurcation and pattern amplitude near onset

The maximum amplitude of the convective flow field is equivalent to the amplitude of the pattern A. We measured the y component of the flow velocity as a function of applied voltage V for a film 45 layers thick. The wavelength of the pattern did not change over the range of V studied. Figure 6 shows the maximum amplitude of v_y, measured at $y \simeq 1/2$ far from the sidewalls, as a function of the control parameter $\epsilon = V^2/V_c^2 - 1$ [13,15,16]. The data show a slightly imperfect supercritical bifurcation at $\epsilon = 0$ at which the motionless state loses stability to the convecting state. Above the bifurcation, the amplitude grows continuously from zero. The curve shown in Fig. 6 is a fit of the data for $\epsilon < 1$ to the steady-state Landau equation, with a constant field f,

$$\epsilon A - gA^3 + f = 0. \tag{3.3}$$

Here the field term accounts qualitatively for the rounding of the data near the bifurcation point, which is due to experimental imperfections. V_c, the nonlinear parameter g, and the field f were used as fit parameters. The fit gave a value of V_c which agreed within experimental uncertainties with the values determined visually and from the film thickness. The agreement between the fit and the data is good, and continues up to $\epsilon \approx 5$, well beyond the range over which one would normally expect the GLE to be applicable. From this fit, $g = (3.2 \pm 0.2) \times 10^{-3}$ s^2/mm^2, and the field parameter $f = 0.15 \pm 0.04$ mm/s. The results change little if f is fixed at zero.

The same data for $\epsilon > 0$ are plotted on logarithmic scales in Figure 7. A simple power-law fit to the data up to $\epsilon = 5$ gives an exponent of 0.48 ± 0.01 and $g = (3.3 \pm 0.1) \times 10^{-3}$ s^2/mm^2. This result is in agreement with the square-root behaviour predicted by Eq. (1.2).

D. Spatial variation of the pattern amplitude

At a rigid wall, the flow velocity, and so the pattern amplitude, must go to zero. Figure 8 shows the absolute value of the velocity component parallel to the electrodes $|v_x|$ measured

at $y \simeq d/5$ and $y \simeq 4d/5$, where $|v_x|$ is largest [13,16]. The amplitude decreases near the end walls, in accordance with the expected boundary condition. The effect of the boundaries on the amplitude extends further into the film at small ϵ, as can be seen by comparing Figures 8(a) ($\epsilon = 0.11$) and 8(b) ($\epsilon = 0.47$).

Figure 9 shows the maximum value of $|v_x|$ for each individual vortex as a function of distance from the end wall for two different values of ϵ. The curves plotted in Figure 9 are fits to Eq. (1.3), with ξ and ϵ/g used as adjustable parameters. Here x and ξ are measured in units of the film width d. The fits describe the data well. ϵ can be determined knowing V_c (or s), and so these fits give a value for g. From measurements on the same three-layer thick film at several values of ϵ, we find $g = 0.59 \pm 0.09$ s^2/mm^2.

In Figure 10, the values of ξ obtained from the same fits are plotted. Fitting the data (with the exception of the point at highest ϵ) to a power law gives

$$\xi/d = (0.36 \pm 0.02)\, \epsilon^{-0.50 \pm 0.02}. \tag{3.4}$$

This result is consistent with the exponent of $-1/2$ predicted by Eq. 1.4, and gives $\xi_0 = 0.36 \pm 0.02$ in units of the film width.

E. Pattern dynamics

The GLE predicts that the evolution of the pattern amplitude A following a sudden change in ϵ should be given by Eq. (1.5). We studied this evolution experimentally by suddenly increasing V from zero to a value above the onset of convection. The maximum value of $|v_x|$ was measured far from the ends of the film as the pattern relaxed to its new steady state.

The results for a film 20 layers thick are shown in Fig. 11, in which the velocity amplitude $|v_x|_{max}$ is plotted as a function of time for two different final values of ϵ. For the larger value of ϵ, the transient change in amplitude happens faster, but the general functional form of the data is the same in both cases.

The curves plotted in Fig. 11 are fits of the data to the solution of the Landau equation, Eq. (1.5). The initial amplitude A_i, ϵ/g, and τ were used as fitting parameters. The fits describe the evolution of the pattern amplitude well. From several such fits, and using the onset voltage to calculate ϵ, we find $g = 0.23 \pm 0.05$ s^2/mm^2 for this film.

Fig. 12 shows the reciprocal of the relaxation time τ as a function of the final value of ϵ for the same film. A fit to a straight-line through the origin gives

$$\tau^{-1} = (1.98 \pm 0.06)\,\epsilon, \tag{3.5}$$

where τ is measured in seconds. This behaviour is consistent with the prediction of Eq. 1.6, and gives $\tau_0 = 0.505 \pm 0.015$ s. A fit of the same data to a power law gives an exponent of -1.12 ± 0.03, consistent with the expected exponent of -1.

IV. DISCUSSION

In the preceding section, measurements made on electroconvection patterns in freely suspended smectic films were analyzed in terms of the GLE. In all cases, the predictions of the GLE agreed well with the experimental results. The onset of convection occurs via an imperfect supercritical bifurcation, and above onset the pattern amplitude (i.e., the amplitude of the flow velocity) grows like the square root of the control parameter ϵ. The spatial variation of the pattern amplitude near the end walls followed the hyperbolic tangent form obtained by solving the GLE with $A = 0$ at the end wall. The correlation length ξ diverges as $\epsilon^{-0.50\pm0.02}$, in agreement with the $\epsilon^{-1/2}$ divergence predicted from the GLE. The evolution of the amplitude after a sudden change in ϵ was also well described by the functional form obtained from the GLE, and the relaxation time τ diverged as $\epsilon^{-1.12\pm0.03}$, consistent with the predicted ϵ^{-1} behaviour. From the fits to the data presented above, we have determined values of ξ_0, τ_0, and g for our system. We have also measured the onset wave number k_c and the slope of the $V_c(s)$ curve in the thin-film limit.

The theoretical linear stability analysis for this system [15] indicates that distances should be scaled by the film width d. With this scaling, the theory predicts $k_c{}^{theory} = 4.74$, which

is in reasonable agreement with our dimensionless experimental value, $k_c = 4.94 \pm 0.03$. The predicted correlation length, ${\xi_0}^{theory} = 0.285$, is about 20% smaller than the dimensionless experimental value of $\xi_0 = 0.36 \pm 0.02$. In the theory, times are scaled by $\epsilon_0 d/\sigma s$. Here ϵ_0 is the permittivity of free space and σ is the conductivity of the doped 8CB in the plane of the film. With this scaling, the theory predicts ${\tau_0}^{theory} = 0.351$. Unfortunately, σ is less well known than the geometric factors d and s. From dc measurements [26], σ is estimated to be $(3.3 \pm 0.1) \times 10^{-7}$ $(\Omega\mathrm{m})^{-1}$, while at 1 kHz the measured value of σ is [27] $(1.11 \pm 0.09) \times 10^{-7}$ $(\Omega\mathrm{m})^{-1}$. The difference may be due to electrochemical effects that occur at the electrodes at dc. The dc value of σ gives a dimensionless experimental τ_0 which is 70% larger than ${\tau_0}^{theory}$, while the 1kHz σ gives a value which is 40% smaller. If we regard σ as a fitting parameter, agreement with ${\tau_0}^{theory}$ requires $\sigma = \sigma^{fit} = (2.0 \pm 0.2) \times 10^{-7}$ $(\Omega\mathrm{m})^{-1}$.

The theory also predicts the onset voltage $V_c = (R_c \sigma \eta)^{1/2} s/\epsilon_0$, where $R_c \approx 77$ is a constant and η is the viscosity component appropriate for shears in the layer planes. We do observe the predicted proportionality between V_c and s, for small s. η is not well known, but by extrapolating measurements made on pure 8CB in the higher temperature nematic phase [29], we estimate $\eta = 0.041 \pm 0.008$ kg/m s. Using σ^{fit} and this value of η, the predicted value of V_c/s is about a factor of four smaller than we measured. Conversely, fixing $\sigma = \sigma^{fit}$ and using η as a fitting parameter, we find $\eta = \eta^{fit} = 0.75 \pm 0.04$ kg/m s. The theory neglects air drag on the film, which is likely to be significant for thin, fast moving films [28]. It is unclear if drag is sufficient to explain the very large value of η^{fit}, however.

The nonlinear parameter g cannot be calculated from the linear stability analysis. However, the dimensions of g are such that it should be scaled by ${\epsilon_0}^2/\sigma^2 s^2$. With this scaling, and using $\sigma = \sigma^{fit}$, we get $g = 0.034 \pm 0.007$ from the pattern amplitude as a function of ϵ, and $g = 0.027 \pm 0.007$ from the spatial variation of A. These values are consistent with each other within the uncertainties. The value obtained from the measurements of the amplitude following a sudden change in applied voltage was substantially higher, $g = 0.47 \pm 0.14$. The reason for the discrepancy is not known, but may be related to air drag effects.

The GLE has not been derived from the electrohydrodynamic equations of motion for

this system [15]. However, one would expect the GLE to apply to any one-dimensional pattern forming system which has translational symmetry in the base state and is periodic and reflection-symmetric in the pattern state [8]. The results presented here confirm this expectation and demonstrate that the behaviour of electroconvection patterns in smectic films can be understood in terms of this much-studied amplitude equation.

ACKNOWLEDGMENTS

We are grateful to Z. Daya and T. Molteno for many useful discussions, and to J. Gleeson for measuring the conductivity of our liquid crystal sample. This research was funded by the Natural Sciences and Engineering Research Council of Canada.

REFERENCES

[1] M.C. Cross and P.C. Hohenberg, Rev. Mod. Phys. **65**, 851 (1993).

[2] H.L. Swinney and J.P. Gollub, *Hydrodynamic Instabilities and the Transition to Turbulence* (Springer, Berlin, 1984).

[3] F. Melo, P.B. Umbanhowar, and H.L. Swinney, Phys. Rev. Lett. **75**, 3838 (1995).

[4] Q. Ouyang and H.L. Swinney, Chaos **1**, 411 (1991).

[5] K.J. Lee, E.C. Cox, and R.E. Goldstein, Phys. Rev. Lett. **76**, 1174 (1996).

[6] A.C. Newell and J.A. Whitehead, J. Fluid Mech. **38**, 279 (1969).

[7] L.A. Segel, J. Fluid Mech. **38**, 203 (1969).

[8] G.H. Gunaratne, Chaos, Solitons and Fractals **5**, 1447 (1995); G.H. Gunaratne, Q. Ouyang, and H.L. Swinney, Phys. Rev. E **50**, 2802 (1994).

[9] R. Graham and J.A. Domaradski, Phys. Rev. A **26**, 1572 (1982).

[10] A. Aitta, G. Ahlers, and D.S. Cannell, Phys. Rev. Lett. **54**, 673 (1985).

[11] G. Ahlers, in *Lectures in the Sciences of Complexity,* edited by D. Stein (Addison, Reading, MA, 1989), p. 175.

[12] S.W. Morris, J.R. de Bruyn, and A.D. May, Phys. Rev. Lett. **65**, 2378 (1990); J. Stat. Phys. **64**, 1025 (1991).

[13] S.W. Morris, J.R. de Bruyn, and A.D. May, Phys. Rev. A **44**, 8146 (1991).

[14] S.S. Mao, J.R. de Bruyn, Z.A. Daya and S.W. Morris, unpublished

[15] Z.A. Daya, S.W. Morris, and J.R. de Bruyn, unpublished.

[16] S.S. Mao, M.Sc. thesis, Memorial University of Newfoundland, 1996 (unpublished).

[17] M.C. Cross, P.G. Daniels, P.C. Hohenberg, and E.D. Siggia, Phys. Rev. Lett. **45**, 898

(1980); J. Fluid Mech. **127**, 155 (1983).

[18] R.P. Behringer and G. Ahlers, Phys. Lett. **62**, 329 (1977).

[19] J. Wesfreid, Y. Pomeau, M. Dubois, C. Normand, and P. Bergé, J. Phys. (Paris) **39**, 725 (1978).

[20] J.P. Gollub and M.H. Freilich, in *Fluctuations, Instabilities, and Phase Transitions*, edited by T. Riste (Plenum, New York, 1974).

[21] P.G. de Gennes and J. Prost, *The Physics of Liquid Crystals, 2nd ed.* (Clarendon, Oxford, 1993).

[22] E.B. Sirota, P.S. Pershan, L.B. Sorensen, and J. Collett, Phys. Rev. A **36**, 2890 (1987).

[23] Committee on Colorimetry, Optical Society of America, in *The Science of Color* (Crowell, New York, 1963).

[24] C. Rosenblatt and N. Amer, Appl. Phys. Lett. **36**, 432 (1980).

[25] M. Born and E. Wolf, Principles of Optics (Pergamon, New York, 1975).

[26] Z.A. Daya, unpublished.

[27] J.T. Gleeson, private communication.

[28] Y. Couder, J.M. Chomaz, and M. Rabaud, Physica **D37**, 406 (1989).

[29] H. Kneppe, F. Schneider, and N.K. Sharma, Ber. Bunsenges. Phys. Chem. **85**, 784 (1981).

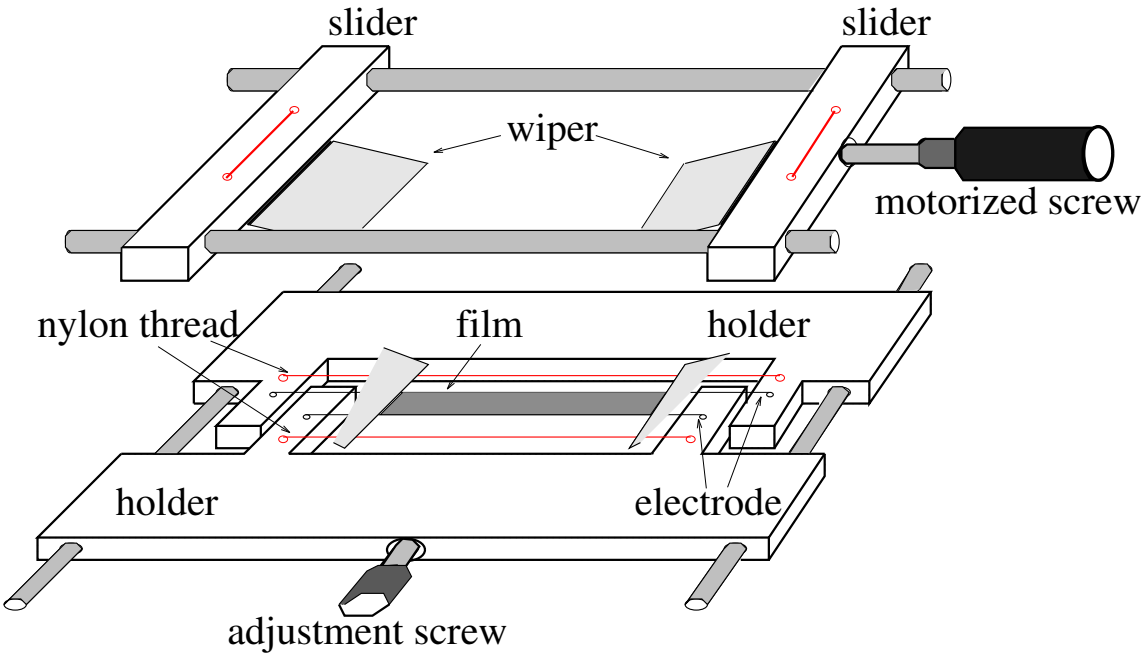

FIG. 1. Diagram of the film holder used in the experiments.

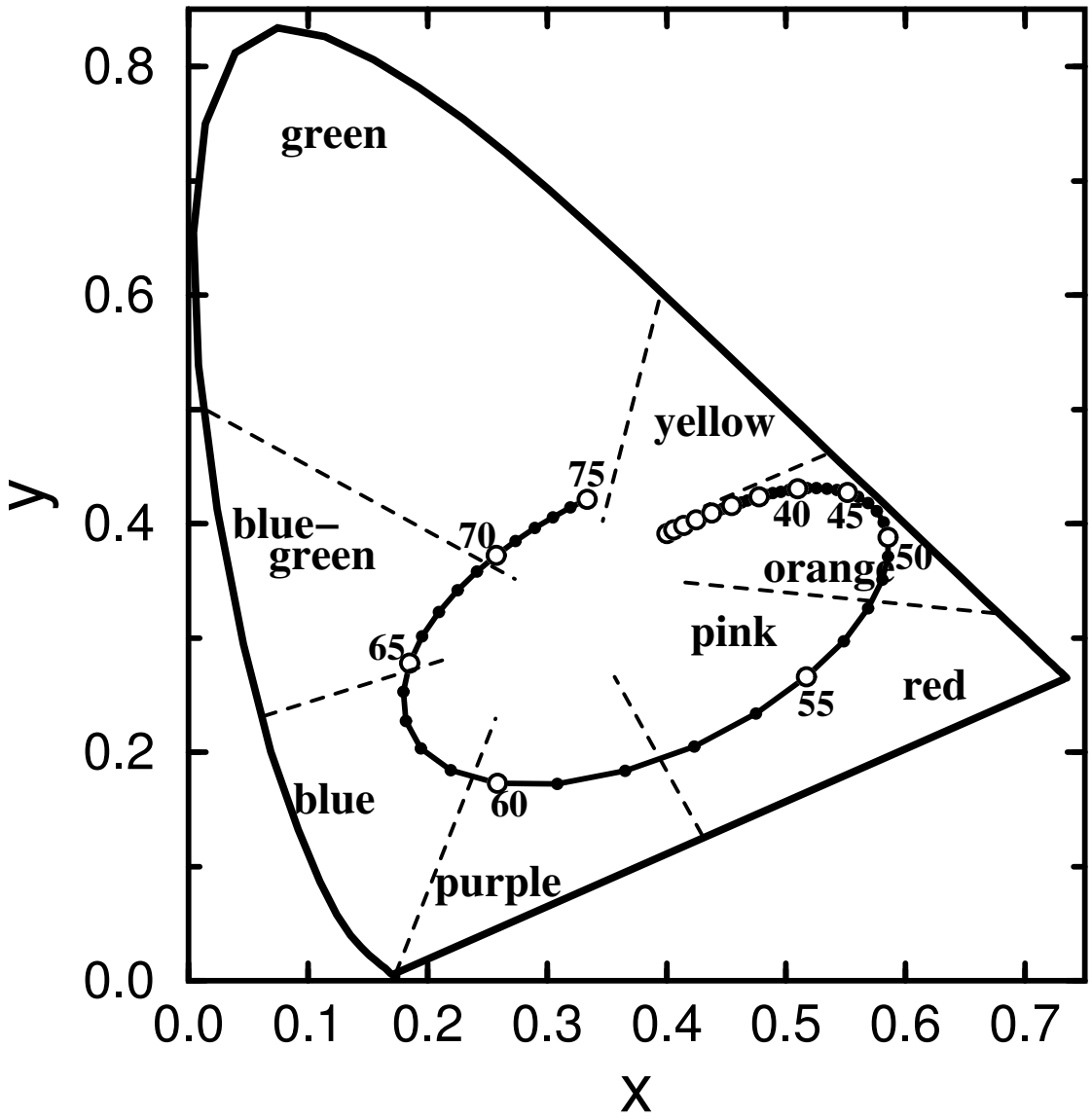

FIG. 2. The calculated colour of 8CB films illuminated by a CIE standard source A at normal incidence, plotted on a CIE chromaticity diagram. Here the axes are CIE chromaticity coordinates, and the numbers on the diagram give the film thickness in molecular layers.

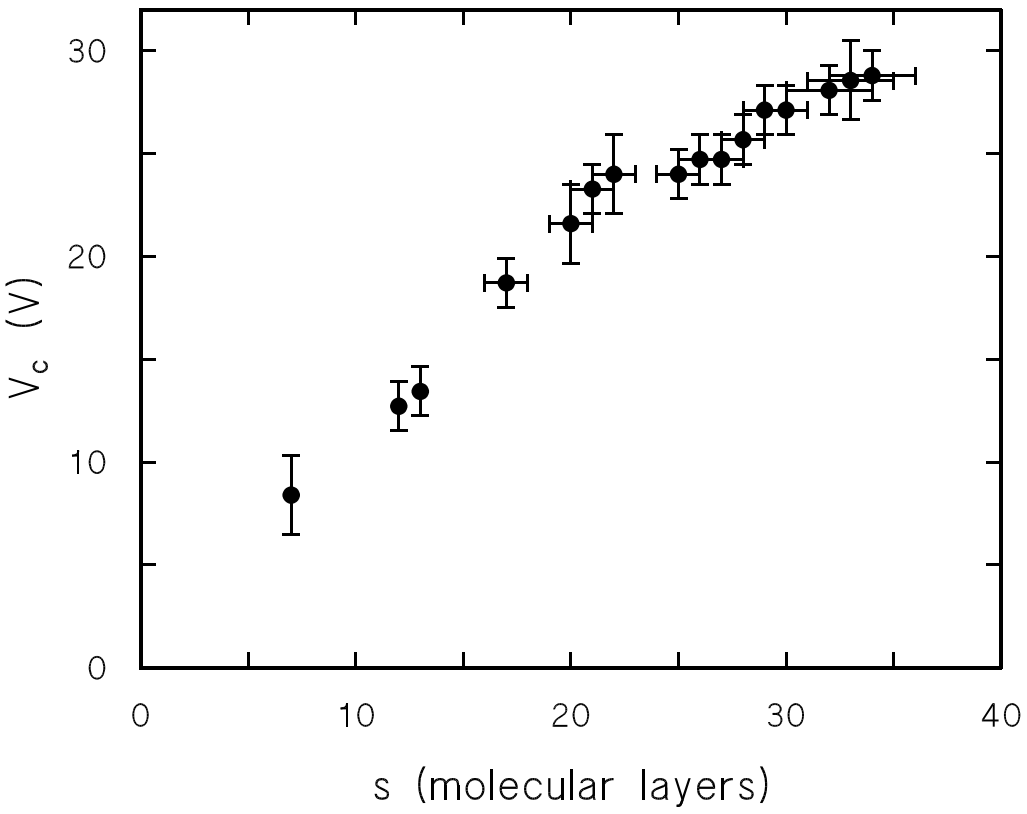

FIG. 3. The onset voltage V_c as a function of film thickness for films 20.0 mm by 2.0 mm.

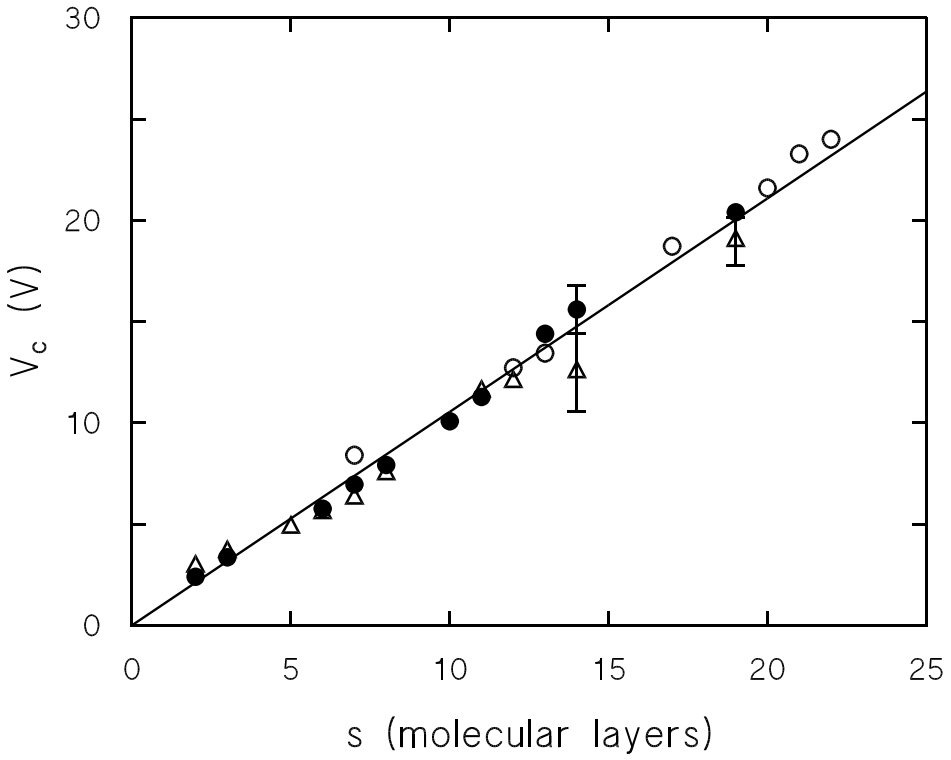

FIG. 4. Onset voltage as a function of film thickness for very thin films of three different sizes. Solid circles: 10.0 mm by 0.7 mm; open circles: 20.0 mm by 2.0 mm; open triangles: 15.0 mm 1.0 mm. The line is a fit through the origin to all of the data.

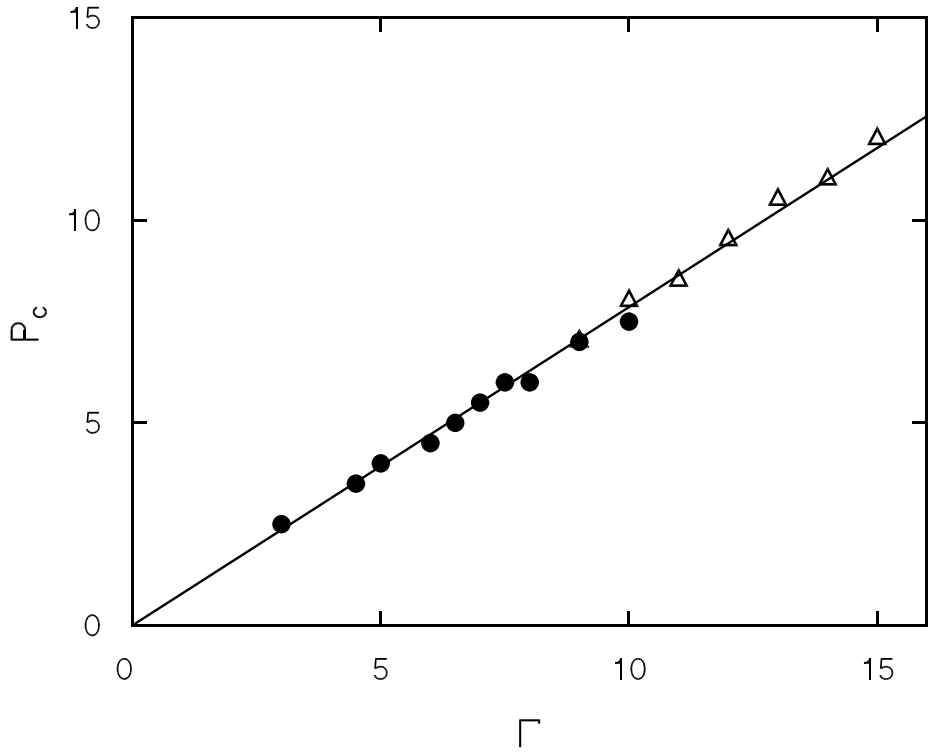

FIG. 5. The number of vortex pairs at the convective onset P_c as a function of aspect ratio Γ. The open triangles were measured on films 1.0 mm wide, and the solid circles on films 2.0 mm wide. The solid line is a linear fit through the origin to both sets of data.

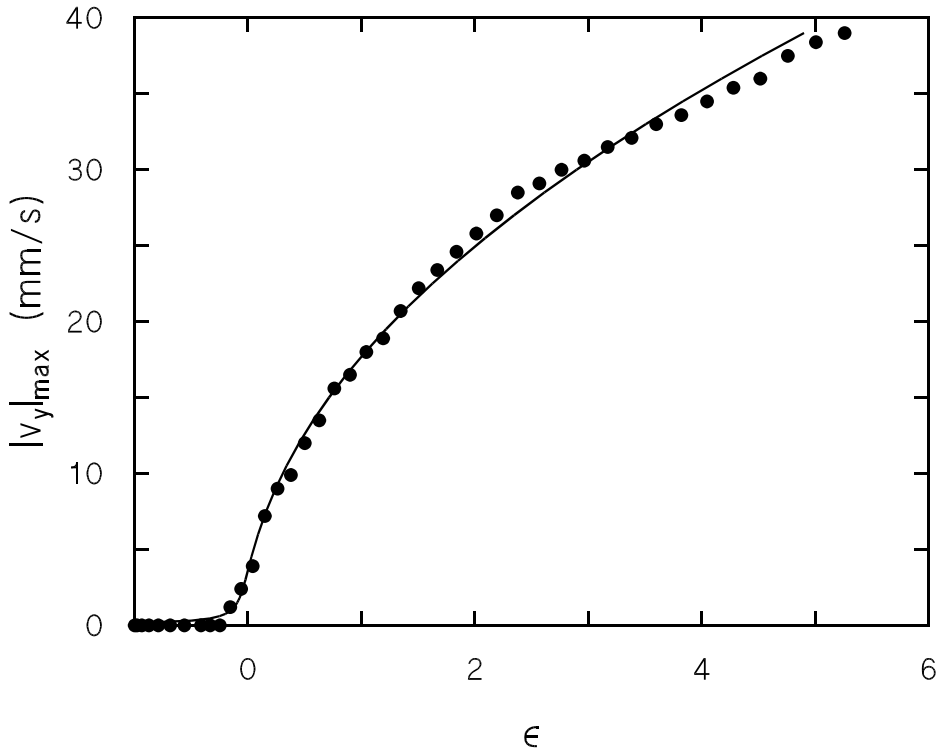

FIG. 6. The maximum value of $|v_y|$ as a function of the dimensionless control parameter ϵ. The curve is a fit of Eq. (3.3) to the data for $\epsilon < 1$. The film used here was 20mm by 2.0 mm and 45 molecular layers thick.

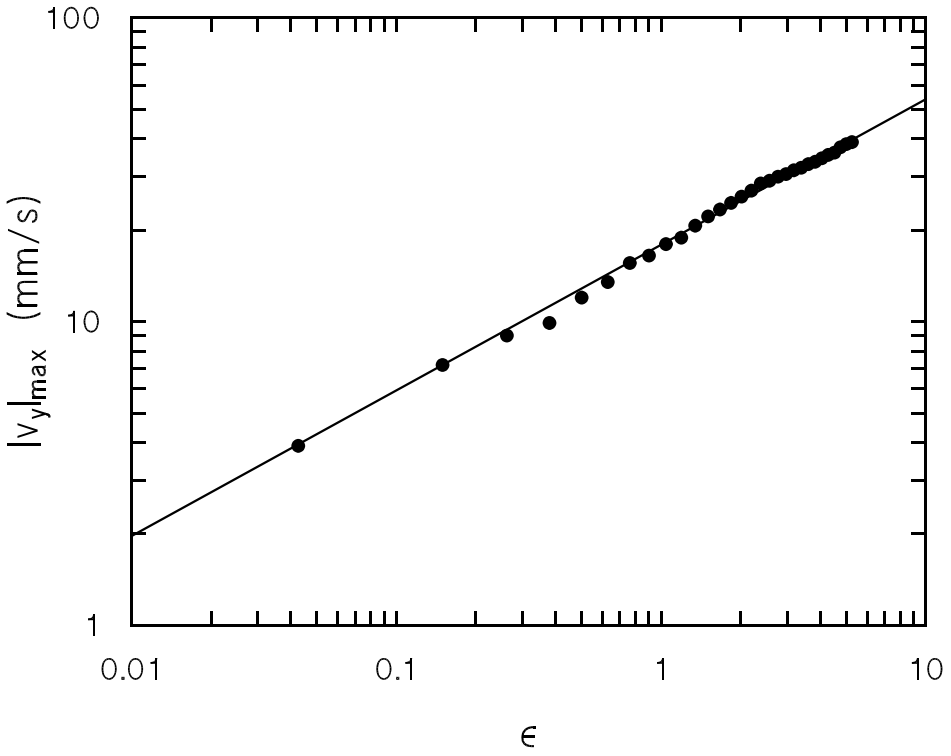

FIG. 7. The data of Fig. 6 for $\epsilon > 0$ plotted against ϵ with logarithmic axes. The line is a fit to all of the plotted data.

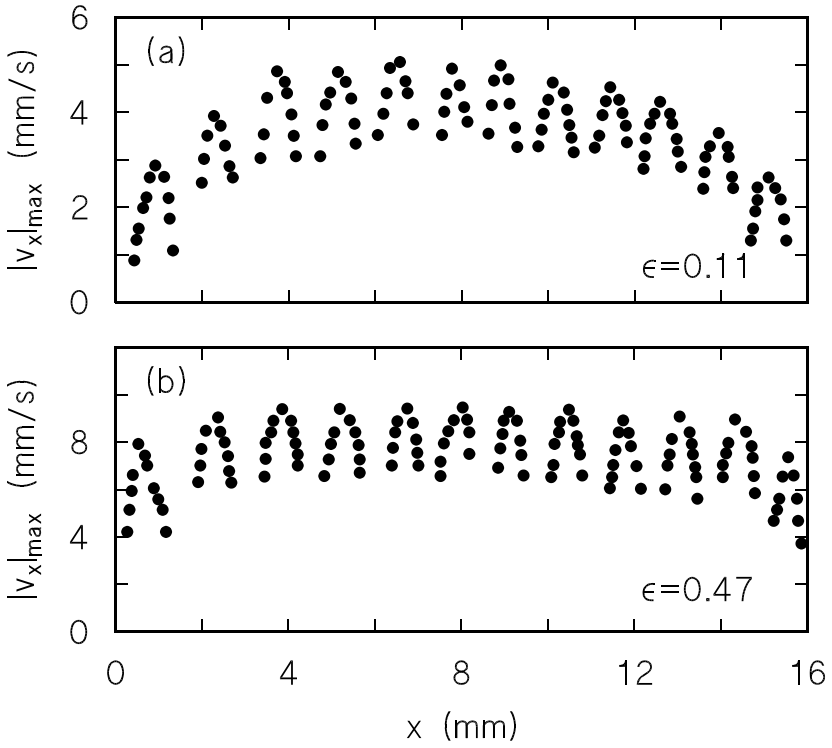

FIG. 8. $|v_x|$ as a function of position along the length of a film for two values of ϵ. Convection is suppressed near the end walls. The film had dimensions 16.0 mm by 2.0 mm.

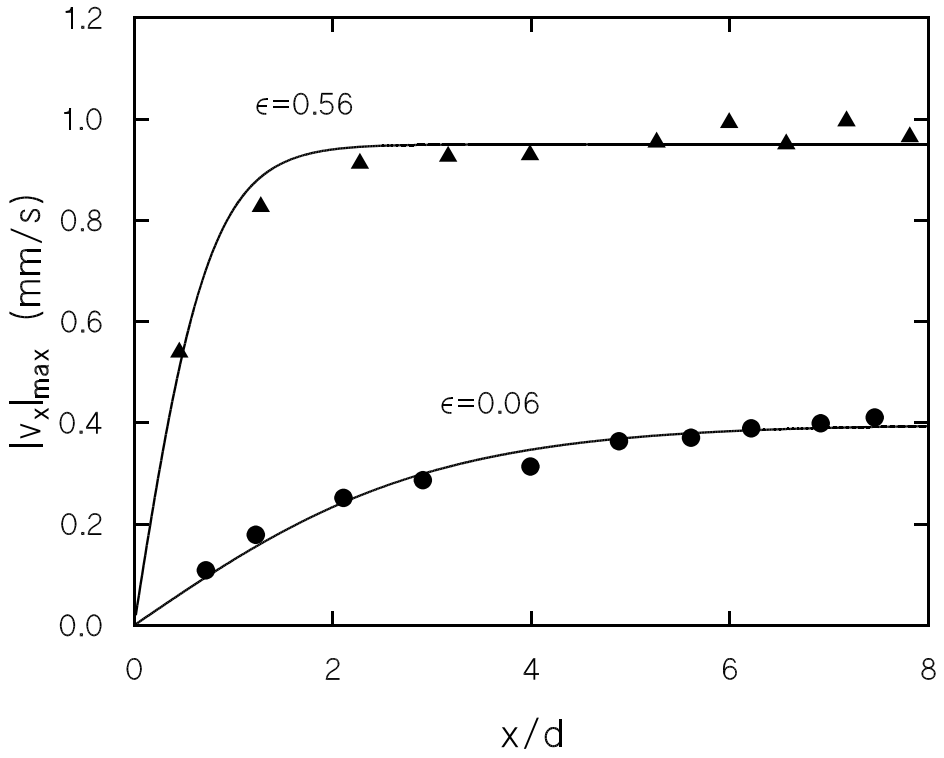

FIG. 9. The maximum value of $|v_x|$ in each vortex as a function of distance from the sidewall for two values of ϵ. The curves are fits of Eq. 1.3 to the data. The film had dimensions 10.0 mm by 0.66 mm and was 3 molecular layers thick.

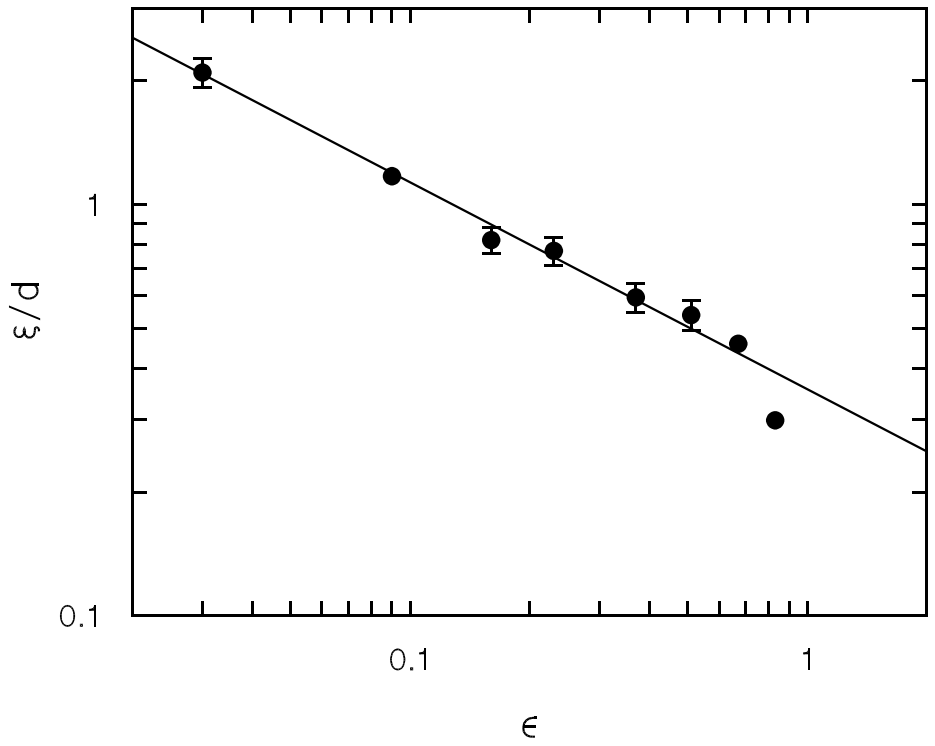

FIG. 10. The length scale ξ, determined using the same film as in Fig. 9, as a function of ϵ. The line is a fit to the data.

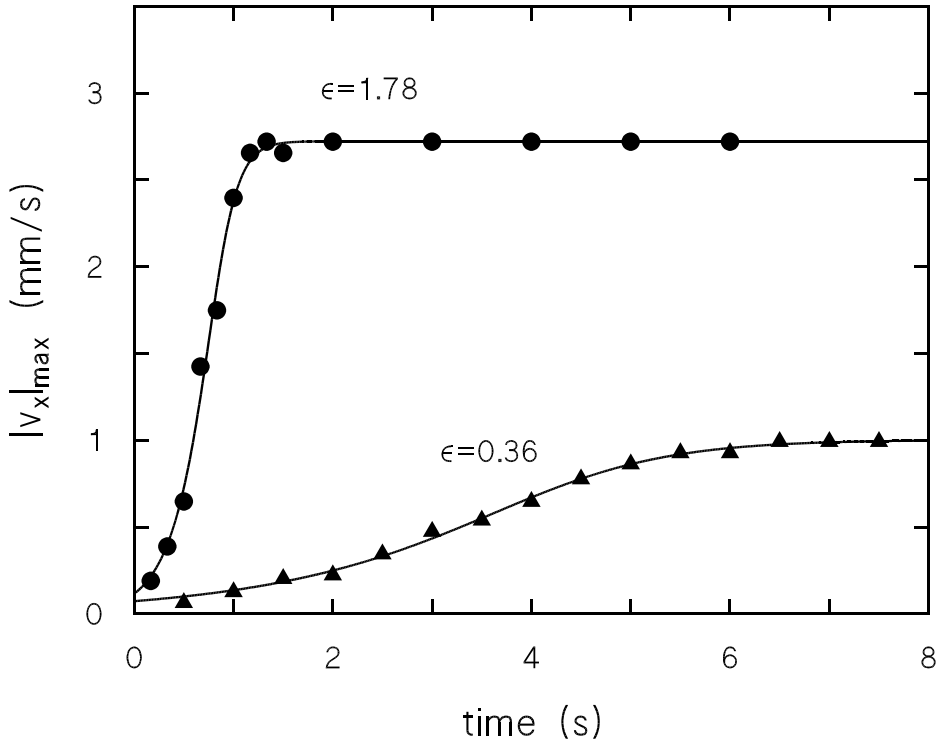

FIG. 11. Evolution of the velocity amplitude after a sudden change of the voltage across the film from zero to a supercritical value. The curves are fits of Eq. 1.5 to the data. The film thickness was 20 molecular layers.

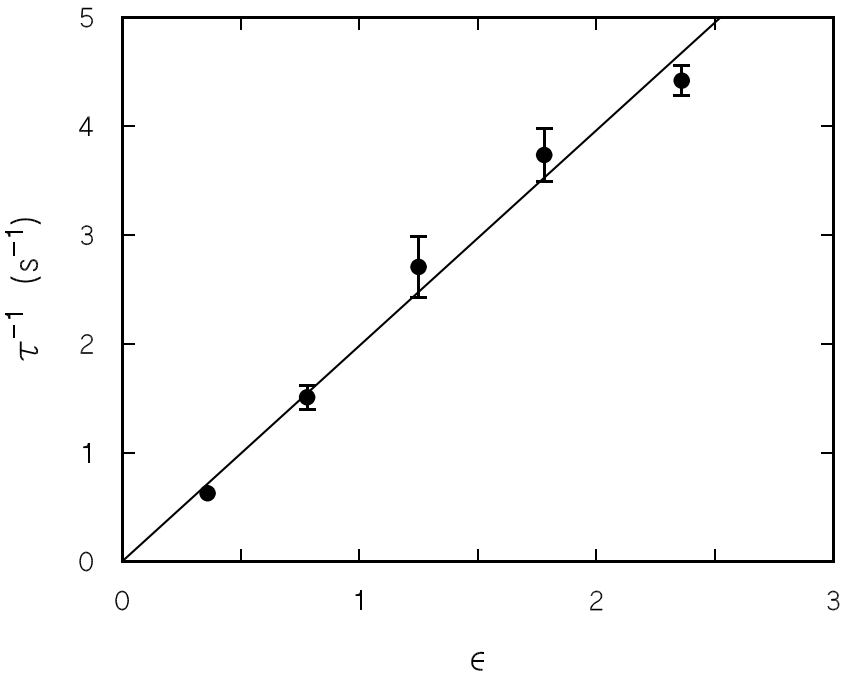

FIG. 12. The growth rate $1/\tau$ as a function of the final value of ϵ. The line is a fit through the origin to the data.